# Physical mechanisms of fatigue in neat polyamide

*E. Mourglia-Seignobos[1], D. Long[1], L. Odoni, P. Sotta[1], L. Vanel[1], C. Rochas[2], T. Narayanan[2]*

1: LPMA, CRTL, 85 rue des frères Perret, BP62, 69192 SAINT-FONS Cedex, France

2: ESRF, Beamline ID2, 6 rue Jules Horowitz, BP220, 38043 Grenoble Cedex, France

February 28, 2011

## 1. Introduction

Semi-crystalline polymers show high mechanical performances and find numerous industrial applications. They are now well characterized. Their crystalline morphology is complex and multi-scale [1-3]. It is composed of a lamellar crystalline phase and an amorphous phase between the lamellae. The typical thickness of a polymer lamella is about 10 nm. The lamellae grow radially from a nucleus in the molten polymer. At a mesoscopic scale, the crystalline phase forms spherulites of a diameter from microns to tens of microns. The mechanical behaviour of semi-crystalline polymers has been widely studied [4-7].

However, the mechanical behaviour in the case of repeated small stresses (fatigue) is still poorly understood. Understanding the mechanisms of damage in semi-crystalline polymers is of great importance, because the stress at break in fatigue is much lower that in tensile solicitation. The mechanical properties of the polymers submitted to fatigue drop as a function of the test duration, even for a maximum stress in the elastic or viscoelastic domain. The irreversible damage which occurs at small stresses during fatigue has not been completely characterized and understood [12-21]. Some works dealt with the study of the mechanical properties at a macroscopical scale[22], some other studied used microscopical observations [23,24], and some others did both [25-28]. Kuksenko and Tamusz have studied damage mechanisms in polymers in situ by SAXS[29] during tensile experiments. They show the

formation of microvoids (cavities) with constant size. Breaking occurs when a critical density of microvoids is reached. Cavity sizes are a few tens of nanometers in oriented polymers and a few thousands of nanometers in non oriented polymers. Recently, Castagnet characterized PVDF by volumetric measurements during tensile test and by SAXS [30]. It was shown that cavities occur in the interlamellar amorphous phase just before yielding. Pawlak and Galeski studied cavitation and crystal shearing in polyamides. Because of the high resistance of the crystals, the main damage mechanism is cavitation [31]. The observed size of the cavities is about 4 to 5 nm. Smaller cavities heal because of the high surface tension of polyamide.

This report shows the results of preliminary SAXS and USAXS experiments performed in order to characterize the fatigue damage in Polyamide. Finally, we will propose a physical model to explain the damage mechanisms on the basis of physical parameters from the material.

## 2. Materials

Polyamide 6,6 (PA66) (obtained by polycondensation of adipic acid and hexamethylenediamine) was used in this study. It was processed in standard conditions to obtain plate specimen (figure 1).

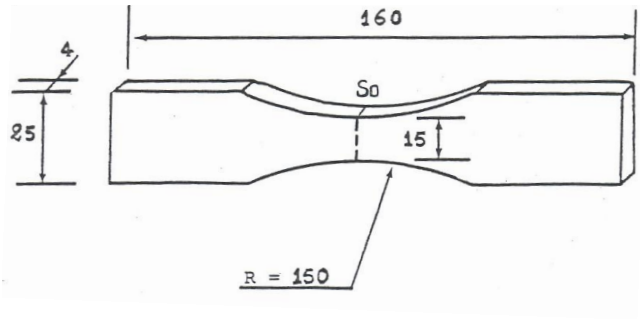


**Figure 1: Specimen geometry used for fatigue tests.**

After moulding, the specimens were stored in sealed bags to maintain them dry as moulded.

The advantage of this geometry is that it localizes damage and minimizes stress concentration (less than 3%).

Test samples were submitted to fatigue tests prior scattering experiments. Fatigue tests consisted of a number $N$ of oscillatory tensile cycles at frequency 5 Hz and characterized by a cyclic ratio $R = \sigma_{min}/\sigma_{max} = 0.1$. The macroscopic properties of the material as a function of the number of cycles during the fatigue test was characterized by following the evolution of the dynamic modulus $E_d$, calculated by the equation $E_d = \frac{(\sigma_{max} - \sigma_{min})}{(\varepsilon_{max} - \varepsilon_{min})}$, and measuring the shape of the fatigue cycles.

Small Angle X-ray Scattering (SAXS) was carried out on the BM2 line at ESRF (Grenoble, France).

The beam wavelength was 0.1110 nm and the pixel size was 1.6016 nm. The distance between the sample and the detector was 1.70 m. The $q$ range was from $q_{max} = 1$ nm$^{-1}$ to $q_{min} = 5 \times 10^{-2}$ nm$^{-1}$. The required time to acquire scattered images was 0.1s (à verifier). This technique is quick enough to carry out in situ tension characterizations.

Ultra Small Angle X-ray Scattering (USAXS) was carried out in the ID2 line at ESRF using the Bonse-Hardt setup. The wavelength of the beam was 0.0995 nm. The $q$ range is from $q_{max} = 5 \times 10^{-2}$ nm$^{-1}$ to $q_{min} = 10^{-3}$ nm$^{-1}$.

For X-ray scattering, the samples were cut with a diamond saw in the central section of the fatigued specimens. In non broken fatigued specimen, we analyzed the middle of the sample. For specimens broken in fatigue, we characterized the area very close to (about 1mm under) the fracture surface.

## 3. Results

### 3.1. Fatigue lifetime

Wöhler curves represent the number of cycles to failure versus the maximum stress. Wöhler curves have been drawn for lifetimes between $10^0$ and $10^{6.5}$ cycles. An example of Wöhler curve is shown in Figure 2.

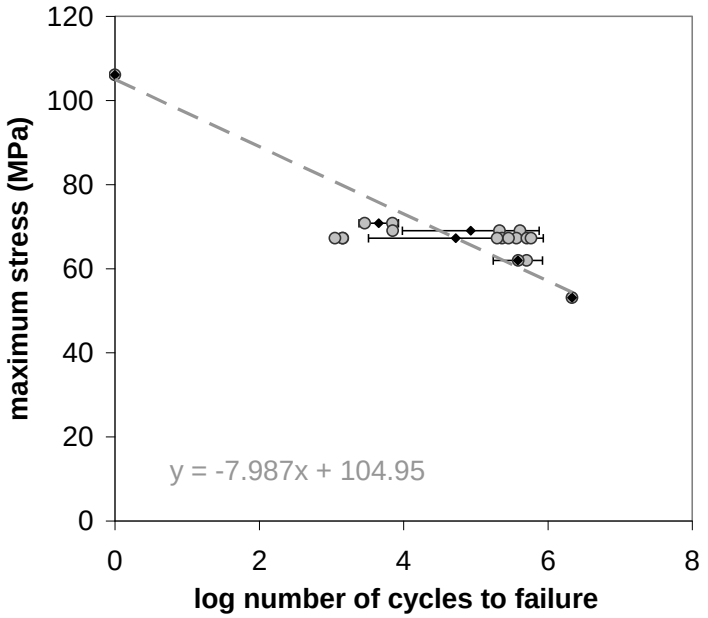


**Figure 2. Wöhler curve for neat PA6,6 at 25°C**

Wöhler curves for neat PA show large standards deviations. There is a linear relationship between the logarithm of the number of cycles to failure and the maximum fatigue stress, as previously shown in the

literature for glass-fiber reinforced PA [18,22,27,32].

The evolution of the dynamic modulus $E_d$ is linear as a function of the number of cycles for neat PA at T < Tg. The relative drop of Ed is large, which indicates generalized damage in the material during fatigue tests.

### 3.2. Microscopic observations

The presence of cavities was first checked by electron microscopy (SEM). The raw (un-fatigued) material show a small number of spherical, randomly located cavities, with an apparent average diameter of about 500 nm. These cavities are most certainly formed during injection moulding, due to thermal retraction of the molten polymer. After fatigue, the number of cavities has increased. The distribution of sizes seems to be large (from 2à nm to several μm in diameter).

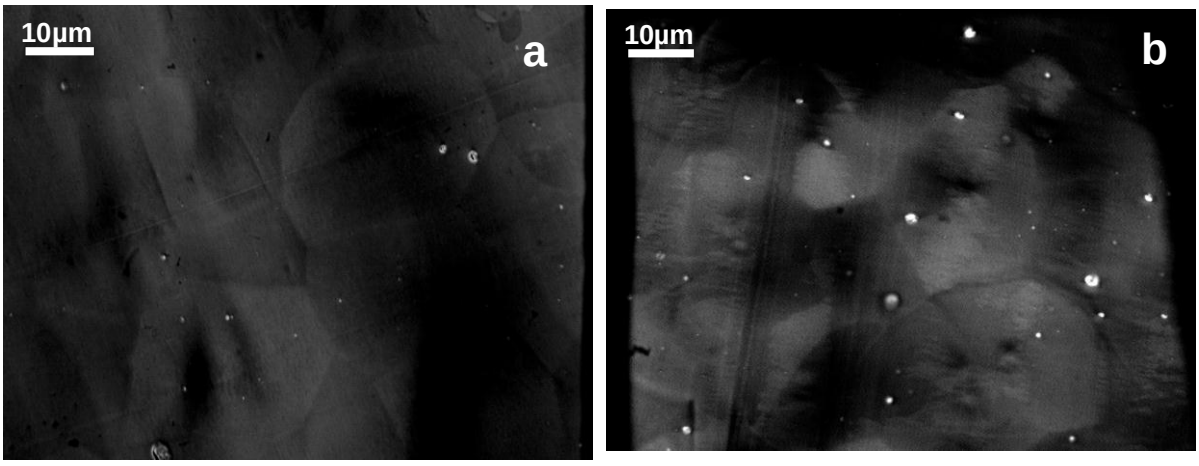


**Figure 3. Observations of polyamides by TEM in a plane parallel to the stress (a) raw (un-fatigued sample); (b) after 300 000 fatigue cycles ($\sigma_{max}$ = 61.9MPa.**

The sample geometry concentrates the stress in a plane located in the middle of the sample. In this zone, cracks are observed up to 150 μm from the failure. We focus here on the characterization of cavities which occur in the bulk of the material

The density of cavities and their distribution of sizes have been estimated by image analysis of TEM pictures along fatigue tests, using ImageJ. Cavities smaller than 100 nm cannot be analyzed quantitatviely. Distributions of sizes of the cavities are shown in **Erreur ! Source du renvoi introuvable.**.

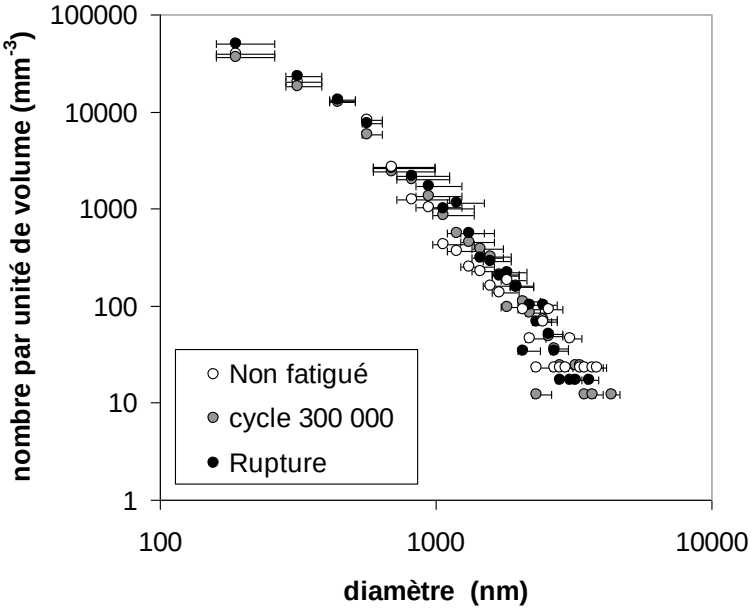


**Figure 4. Evolution de la distribution de taille des cavités sphériques au cours de la fatigue obtenue par analyse d'images sur coupes épaisses de polyamide.**

In all samples, this size distribution seems to follow a power law:

$$n_p(R) = \frac{N_p R^{-\alpha}}{\Delta R}$$

with R the cavity radius (in mm), n(R) the (dimensionless) number of cavities of radius R, ΔR the resolution in size (in mm). Np is a constant to match the ordinate scale. The obtained slope α in fatigued PA is about 3.3. The largest cavities are about 3µm in diameter. The number of cavities of diameter larger than 500 nm is slightly larger in the fatigues sample. This may indicate that large cavities grow during fatigue. Note that the volume fraction of voids is smaller than à 0.1% in the raw material and remains small (0.15%) during fatigue.

### 3.3. Distance between lamellae in the crystallites

SAXS (BM02) were used also to characterize the change in the crystallite morphology (period of the lamellar stacking in the crystallites) during in-situ stretching experiments performed with a home-made stretching device.

The diffraction peak associated to lamellar stacking is located at about 0.7 $nm^{-1}$ (which corresponds to a period of about 9 nm). Thus, XY diffraction patterns recorded in the range 0.1 to 1.2 $nm^{-1}$ and analysed in 36 angular sectors of 10° have allowed us to substract the Porod contribution of the small

angle scattering properly and characterize quantitatively the diffraction peak associated to lamellar stacking. The obtained results show that the lamellar spacing increases perpendicular to the fatigue direction. This indicates that fatigue (in the form of cavities or of zones with a decreased density within the amorphous phase) occurs principally in the equatorial plane of the spherulites (see Figure 1). The obtained results (publication in preparation) are an essential part of the PhD thesis of Elodie Mourglia (MOURGLIA2009).

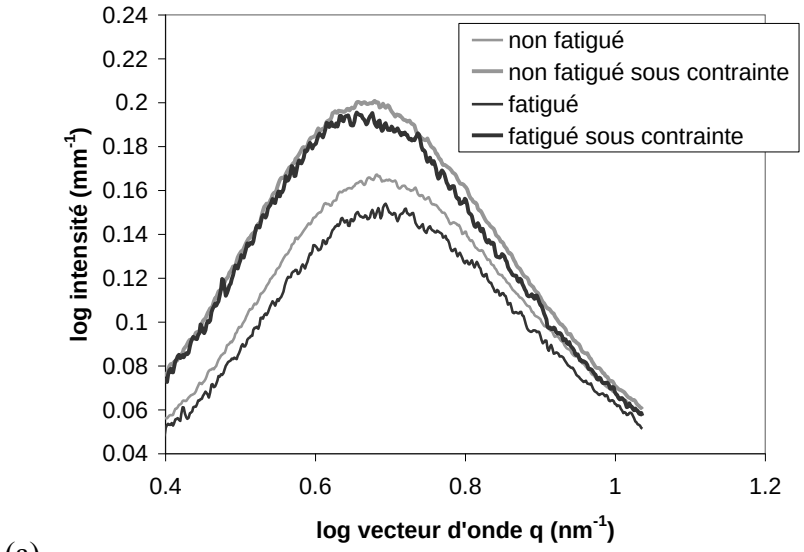


(a)

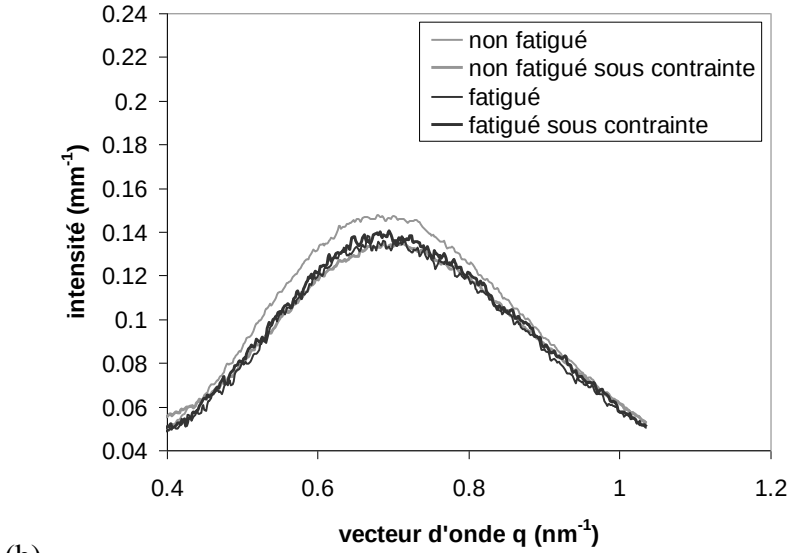


(b)

**Figure 5. Intensité diffusée par les lamelles cristallines dans le polyamide avant et après 300 000 cycles de fatigue à $\sigma_{max}$=69MPa dans un environnement à 25°C, avec soustraction du signal des cavités (a) direction 90°; (b) direction 0°. Les valeurs de contrainte sont $\sigma_{max}$=50MPa pour le polyamide non fatigué et $\sigma_{max}$=42MPa pour le polyamide fatigué**

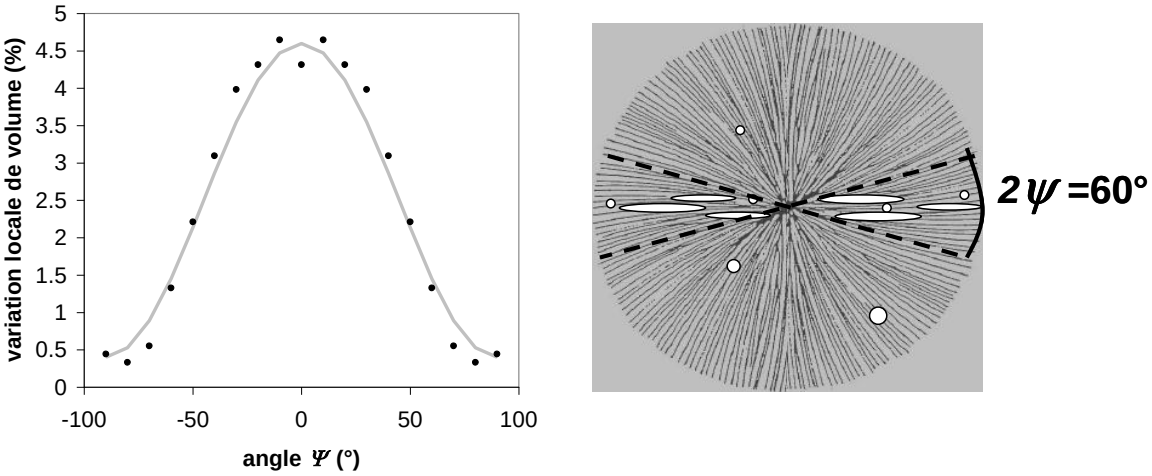


**Figure 6: Variation of the lamellar spacing (expressed in terms of a relative local volume variation) as a function of the angle between lamellae and stretching direction. Corresponding model of damage in equatorial zone of the spherulites**.

| | **U-fatigued** | **Un-fatigued / σ=50MPa** | **fatigued** | **fatigued / σ=42MPa** |
|---|---|---|---|---|
| **position ($nm^{-1}$)** | 0.701 | 0.680 | 0.705 | 0.677 |
| **Repetition distance (nm)** | 8.96 | 9.24 | 8.91 | 9.28 |

### 3.4. Characterization of cavitation by SAXS and USAXS

The distribution of sizes and the volume fraction of the cavities have been characterized during fatigue by analyzing SAXS (BM02) and USAXS (ID02) in the Guinier and Porod regimes. For this, samples were submitted to varying fatigue conditions and durations prior to scattering experiments, and compared to a raw (un-fatigued) reference sample. Samples are submitted to a static tensile stress in order to reopen the cavities formed during fatigue tests.

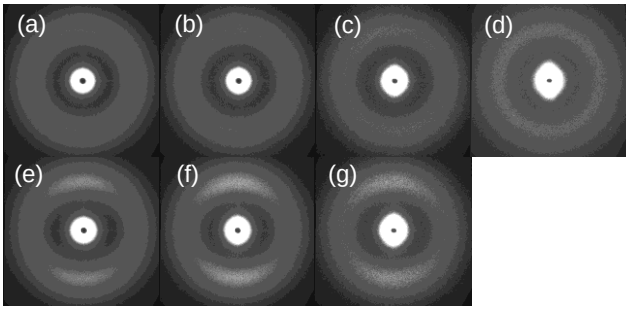


**Figure 7. images de diffusion en SAXS 2D pour le polyamide à différents nombres de cycles en fatigue à 69MPa dans un environnement à 25°C (a) avant fatigue (référence) ; (b) après 2 000 cycles; (c) après 300 000 cycles; (d) à la rupture ; et les mêmes échantillons sous tension (e) référence sous une contrainte à 50MPa; (f) échantillon fatigué 2 000 cycles sous une contrainte de 51MPa; (g) échantillon fatigué 300 000 cycles sous une contrainte de 42MPa. Le sens de traction est vertical**

In order to quantify the size and distribution of sizes of the cavities, we have complemented SAXS experiments (BM02) by USAXS experiments done with a Bonse-Hardt setup (ID02). The quantitative intensity scattered by spherical cavities of radius R and volume V in an homogeneous material is :

$$I(q) = n(R) I_0 T_r \beta^2 (\rho - \rho_0)^2 V^2 \Phi h \left( 3 \frac{(\sin qR - qR\cos qR)}{(qR)^3} \right)^2 \qquad (27)$$

where I(q) is in Wcm2, n(R) is the number of cavities of radius R per unit volume, I0 the incident beam intensity (in W), Tr the sample transmission, β2 the electronic cross section ( $\beta^2 = 7.8 \times 10^{-26} cm^2$ ), Φ the beam size (in cm2), h the sample thickness (in cm), ρ (resp. ρ0) the electronic density of PA (resp. of the cavity) (in cm-3).

Figure 1 shows the normalized intensities for PA samples after various number of fatigue cycles. What is directly obtained in USAXS (after normalizing by sample thickness) is the absolute quantity (expressed here in mm-1) :

$$\frac{I(q)}{I_0 \Phi T_r h} = n(R) \beta^2 (\rho - \rho_0)^2 V^2 \left( 3 \frac{(\sin qR - qR\cos qR)}{(qR)^3} \right)^2 \qquad (54)$$

USAXS spectra have been acquired parallel (a) and perpendicular (b) to the stretch direction.

.

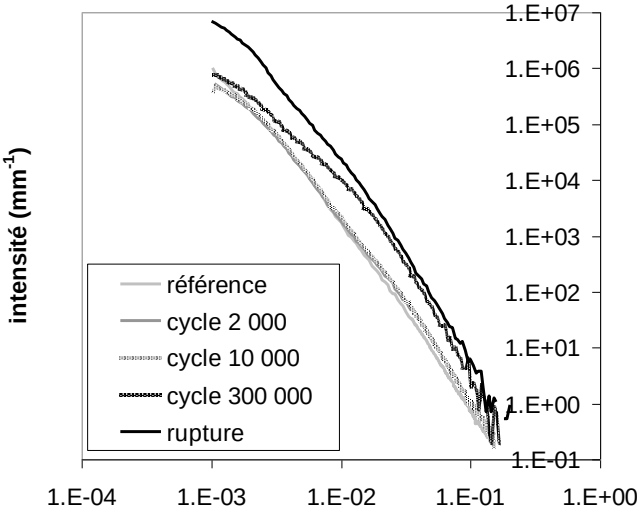


(a)

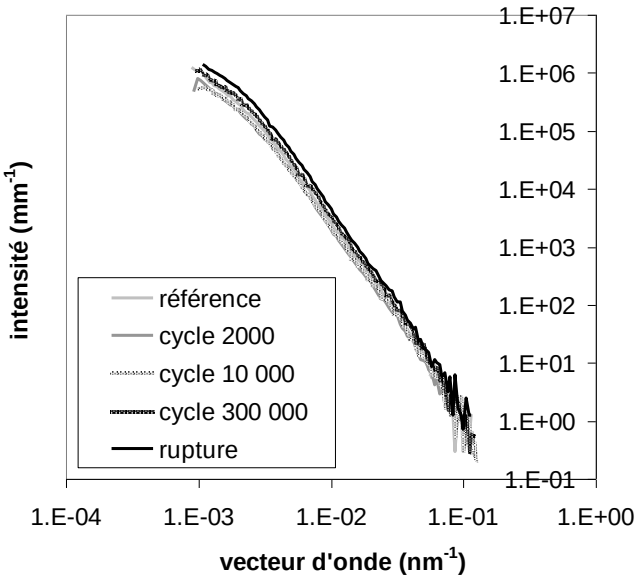


(b)

**Figure 1 : Caractérisations USAXS dans le polyamide fatigué à 69MPa dans un environnement à 25°C (a) direction y ; (b) direction x.**

Figure 1 (a) shows that the scattered intensity increases with the number of fatigue cycles. Below 10000 cycles, the damage is weak and isotropic. The signal is fitted with voids with a distribution of sizes in power law. At larger numbers of cycles, a more intense, anisotropic damage appears. In this new regime, modelling is done with ellipsoidal scattering objects, which are damaged domains with a decreased density as compared to the bulk. Parameters of the model are the dimensions of the objects in the perpendicular direction, their number per unit volume and the volume fraction of PA inside. These parameters are chosen in order to match the variation of the elastic modulus and of the overall density of the material during fatigue cycles. The size distribution is described by a power law:

$$n_p(R) = \frac{N_p R^{-\alpha}}{\Delta R} \qquad (53)$$

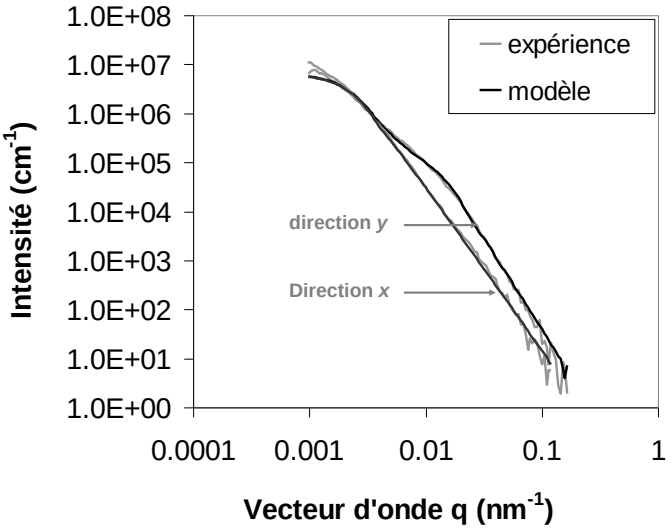


**Figure 2 : Modélisation des intensités diffusées par l'échantillon fatigué 300 000 cycles dans les directions *x* et *y* au moyen de deux lois de puissance.**

| | | *Cavités sphériques formées lors de l'injection* $\xi=0$ | | | | | *Domaines d'endommagement formés en fatigue* $\xi=0.9$ | | | | |
|---|---|---|---|---|---|---|---|---|---|---|---|
| **Nombre de cycles** | $\Delta R$ **(nm)** | $R_{min}$ **(nm)** | $R_{max}$ **(nm)** | $N_P$ **(cm$^{-2+\alpha}$)** | $\alpha$ | $\varphi$ | $R_{min}$ **(nm)** | $R_{max}$ **(nm)** | $N_P$, **(cm$^{-2+\alpha}$)** | $\alpha$ | $\varphi$ |
| 0 | 20 | 10 | 1350 | $4\ 10^{-9}$ | 3.6 | 1 | - | - | - | - | - |
| $2.10^3$ | 20 | 10 | 1230 | $3.5\ 10^{-9}$ | 3.6 | 1 | 10 | 110 | $1.0\ 10^{-1}$ | 2.5 | 1 |
| $1.10^4$ | 20 | 10 | 1290 | $3.5\ 10^{-9}$ | 3.6 | 1 | 10 | 110 | $1.5\ 10^{-1}$ | 2.5 | 1 |
| $3.10^5$ | 20 | 10 | 1190 | $6\ 10^{-9}$ | 3.6 | 1 | 10 | 190 | $1.5\ 10^{-3}$ | 2.5 | 5 |
| rupture | 20 | 10 | 1300 | $16\ 10^{-9}$ | 3.6 | 1 | 10 | 190 | $2.5\ 10^{-3}$ | 2.5 | 5 |
| | | | | | | | 10 | 1310 | $1.3\ 10^{-4}$ | 2.5 | 5 |

**Figure 3 : Paramètres de modélisation des spectres de diffusion dans le PA.**

An example of modelling of the signal is given in figure 8.

| **Nombre de cycles** | *$V_P$ (domaines d'endommagement en fatigue)* **(%)** |
|---|---|
| 0 | - |
| $2.10^3$ | 0.51 |
| $1.10^4$ | 0.76 |
| $3.10^5$ | 0.43 |
| rupture | 1.4 |

**Figure 4 : Fractions volumiques de la population de cavités sphériques liées au moulage par injection et de la population des domaines d'endommagement en fatigue.**

| | | *Domaines d'endommagement formés en fatigue* $\xi$=0.83 | | | | | |
|---|---|---|---|---|---|---|---|
| **Nombre de cycles** | $\Delta R$ **(nm)** | $2\psi$ **(°)** | $R_{min}$ **(nm)** | $R_{max}$ **(nm)** | $N_P$, **(cm$^{-2+\alpha}$)** | $\alpha$ | $\varphi$ |
| 0 | 20 | - | - | - | - | - | - |
| $2.10^3$ | 20 | 60 | 10 | 110 | $1.0\ 10^{-1}$ | 2.5 | 1 |
| $1.10^4$ | 20 | 60 | 10 | 110 | $1.5\ 10^{-1}$ | 2.5 | 1 |
| $3.10^5$ | 20 | 60 | 10 | 190 | $1.5\ 10^{-3}$ | 2.5 | 5 |
| rupture | 20 | 60 | 10 | 190 | $2.5\ 10^{-3}$ | 2.5 | 5 |
| | | 60 | 10 | 1310 | $1.3\ 10^{-4}$ | 2.5 | 5 |

**Figure 5 : Paramètres de modélisation des spectres de diffusion dans le PA.**

| **Nombre de cycles** | $V_P$ *(domaines d'endommagement en fatigue)* **(%)** |
|---|---|
| 0 | - |
| $2.10^3$ | 0.17 |
| $1.10^4$ | 0.25 |
| $3.10^5$ | 0.14 |
| rupture | 0.47 |

**Figure 6 : Evolution des fractions volumiques des domaines d'endommagement en fonction du nombre de cycles de fatigue.**

En tenant compte de la corrélation spatiale des domaines d'endommagement, on explique la chute du module à rupture présentée au chapitre 4 par la présence de domaines anisotropes orientés perpendiculairement à la contrainte et contenant 83% de matière.

Des caractérisations par diffusion des rayons X aux très petits angles nous ont permis de montrer la nucléation de domaines d'endommagement nanométriques sphériques dans le polyamide, d'un diamètre caractéristique de 20 à 220nm. Durant les premiers stades de la fatigue, nous avons montré que le nombre de ces nanodomaines augmente avec le nombre de cycles de fatigue, mais que leur taille reste constante. La nucléation de ces nanodomaines met en jeu plusieurs empilements de lamelles cristallines (dont la distance de répétition caractéristique est d'environ 10nm) et est compatible avec le modèle

proposé par Friedrich. Ensuite certains de ces domaines croissent perpendiculairement à la contrainte. Dans le polyamide nous supposons donc que les craquelures soient initiées préférentiellement par la nucléation de nanodomaines dans la phase amorphe entre lamelles cristallines orientées perpendiculairement à la contrainte, comme présenté dans la partie bibliographique dans le poly(fluorure de vinylidène) [30]. A la rupture les domaines elliptiques ont une taille comprise entre 20nm et 2.6µm parallèlement à la contrainte, et comprise entre 20nm et 13.1µm perpendiculairement à la contrainte. Pour comparer avec la littérature des polymères semi-cristallins non orientés, on peut rappeler que Kuksenko et Tamusz ont observé des cavités d'un diamètre de plusieurs centaines de nanomètres sous déformation [29].

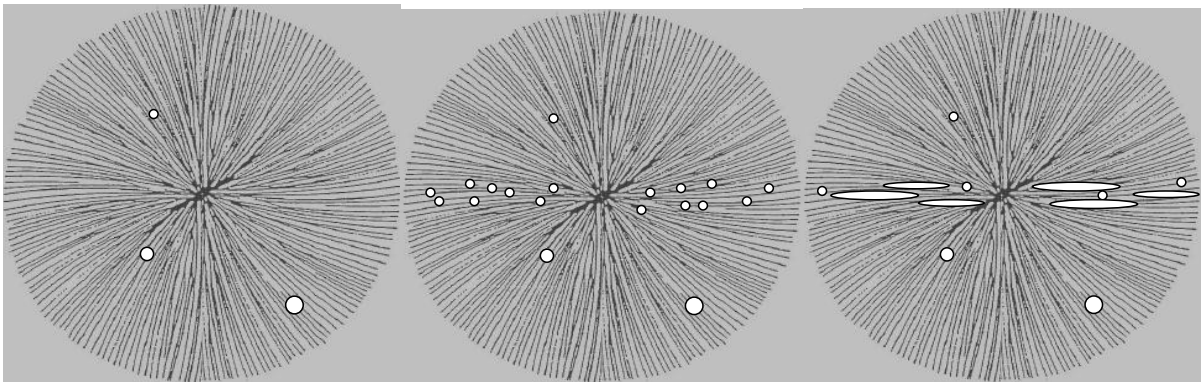

**Figure 7 : Croissance des cavités submicroniques dans la phase amorphe entre les lamelles orientées perpendiculairement à la contrainte (a) cavités microniques de large distribution de taille dans l'échantillon non fatigué; (b) nucléation de cavités nanométriques dans la phase amorphe entre lamelles perpendiculaires à la contrainte (diamètre entre 20 et 180nm environ) ; (c) augmentation du nombre de ces cavités sphériques nanométriques ; (d) et (e) croissance des cavités nanométriques dans la direction perpendiculaire à la contrainte.**

Les cavités sphériques liées à la mise en œuvre n'explique pas l'évolution des propriétés mécaniques mais contribue certainement à l'endommagement. En effet, comme détaillé dans la littérature [8,38]. La présence des cavités sphériques microniques suite à la mise en œuvre par injection cause une forte concentration locale de la contrainte macroscopique et favorise sans doute la nucléation des cavités submicroniques.

## 4. Physical model

We have proposed a physical model of damage mechanisms in the regime of logarithmic evolution of the elastic modulus, before the final catastrophic regime of failure.

Le polyamide est un matériau semi-cristallin et donc hétérogène par nature. La déformation est donc

localement hétérogène. Ainsi la déformation macroscopique est amplifiée localement et l'amplification locale de la déformation présente un intervalle très large. On considère que toute l'hétérogénéité du système est exprimée par l'hétérogénéité de déformations locales. On note cet intervalle d'amplifications locales [μ- ; μ+] et dans cet intervalle on définit une probabilité d'amplification p(μ). Cette notion d'hétérogénéités de déformations locales est équivalente à la notion d'hétérogénéités de barrières d'énergie dans un modèle thermiquement activé.

Il est donc possible d'estimer les valeurs du volume d'activation pour les différentes températures d'essai :

$$v(25°C) = 0.6nm^3$$

Le volume d'activation augmente avec la température du matériau, ce résultat a été observé par Holt dans le poly(méthyl méthacrylate) [47]. Les valeurs des volumes d'activation correspondent aux volumes d'activation typiques des mécanismes de plasticité dans les polymères amorphes et semi-cristallins, qui sont compris dans la littérature entre $1nm^3$ et $10nm^3$ [47-51].

## 5. References

Reference List


1. Flory, P. J. Conformations of macromolecules in condensed states. *Pure and Applied Chemistry* **1984,** *56* (3), 305-312.
2. Kohan, M. I. *Nylon Plastic Handbook;* Hanser/Gardner Publications: 1995.
3. Seguela, R. Critical Review of the Molecular Topology of Semicrystalline Polymers: The Origin and Assessment of Intercrystalline Tie Molecules and Chain Entanglements. *Journal of Macromolecular Science, Part B: Physics* **2005,** *43*, 1729-1748.
4. Bowden, P. B.; Young, R. J. Deformation mechanisms in crystalline polymers. *Journal of Materials Science* **1974,** *9* (12), 2034-2051.
5. Brooks, N. W.; Ghazali, M.; Duckett, R. A.; Unwin, A. P.; Ward, I. M. Effects of morphology on the yield stress of polyethylene. *Polymer* **1999,** *40*, 821-825.
6. Brooks, N. W. J.; Duckett, R. A.; Ward, I. M. Effects of crystallinity and stress state on the yield strain of polyethylene. *Polymer* **1999,** *40* (26), 7367-7372.
7. O'Kane, W. J.; Young, R. J.; Ryan, A. J. The Effect of Annealing on the Structure and Properties

of Isotactic Polypropylene Films. *Journal of Macromolecular Science - Part B* **1995,** *B34* (4), 427-458.

15. Hertzberg, R.; Manson, J. *Fatigue of Engineering Plastics;* New York: Academic Press ed.; 1980.

17. Katoh, A.; Handa, K.; Narisawa, I. Damage Behavior in Multi-Stage Fatigue testing of Glass-Fiber-Reinforced Polyamide 66. *Polymer Composites* **2004,** *25* (1), 60-81.

22. Mallick, P. K.; Zhou, Y. Effect of mean stress on the stress-controlled fatigue of a short E-glass fiber reinforced polyamide-6,6. *International Journal of Fatigue* **2004,** *26* (9), 941-946.

23. Horst, J. J.; Spoormaker, J. Mechanisms of Fatigue in Short Glass Fiber Reinforced Polyamide 6. *Polymer Engineering and Science* **1996,** *36* (22), 2718-2726.

26. Bellenger, V.; Tcharkhtchi, A.; Castaing, P. Thermal and mechanical fatigue of a PA66/glass fibers composite material. *International Journal of Fatigue* **2006,** *28* (10), 1348-1352.

29. Kuksenko, V. S.; Tamuzs, V. P. *Fracture micromechanics of polymer materials;* Martinus Nijhoff Publishers ed.; 1981.

30. Castagnet, S.; Girault, S.; Gacougnolle, J. L.; Dang, P. Cavitation in strained polyvinylidene fluoride: mechanical and X-ray experimental studies. *Polymer* **2000,** *41*, 7523-7530.

31. Pawlak, A.; Galeski, A. Plastic Deformation of Crystalline Polymers: The Role of Cavitation and Crystal Plasticity. *Macromolecules* **2005,** *38*, 9688-9697.

37. Glatter, O.; Kratky, O. *Small Angle X-ray Scattering;* Academic Press ed.; 1982.

38. Strobl, G. *The Physics of Polymer;* Springer-Verlag Berlin Heidelberg New York ed.; 2009.